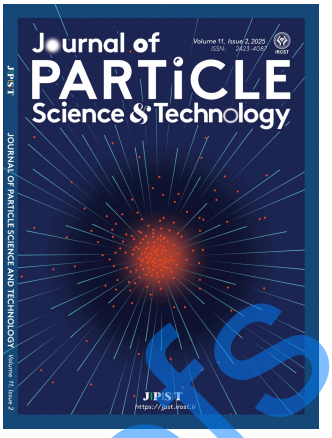
Journal Pre-proofs



Bioactivities of carvacrol-entrapped polycyclodextrin-coated silver nanostructures: Antioxidant, cytotoxic, and antibacterial effects

Elham Gholibegloo, Aseyeh Ghaedi, Sajede Shoja

DOI: https://doi.org/10.22104/jpst.2026.8364.1294
Manuscript number: JPST-2608-1300

To appear in: Journal of Particle Science and Technology (JPST)

Received Date: 22 June 2026
Received Date in revised form: 16 September 2026
Accepted Date: 11 October 2026

Please cite this article as: Gholibegloo, E., Ghaedi, A., Shoja, S., Bioactivities of carvacrol-entrapped polycyclodextrin-coated silver nanostructures: Antioxidant, cytotoxic, and antibacterial effects, *Journal of Particle Science and Technology* (2026), doi: https://doi.org/10.22104/jpst.2026.8364.1294

File of an article that has undergone enhancements after acceptance, such as the addition of a cover page and metadata, and formatting for readability, but it is not yet the definitive version of record. This version will undergo additional copyediting, typesetting and review before it is published in its final form, but we are providing this version to give early visibility of the article. Please note that, during the production process, errors may be discovered which could affect the content, and all legal disclaimers that apply to the journal pertain.

© 2026 The Author(s). Published by IROST.

Journal Pre-proofs

Bioactivities of carvacrol-entrapped polycyclodextrin-coated silver nanostructures: Antioxidant, cytotoxic, and antibacterial effects

Elham Gholibegloo[a,*], Aseyeh Ghaedi[b], Sajede Shoja[a]

[a] *Department of Chemical Technologies, Iranian Research Organization for Science and Technology (IROST), Tehran, Iran*

[b] *Department of Chemistry, Payame Noor University (PNU), Tehran, Iran*

Abstract

The efficient delivery of natural bioactive compounds remains a major challenge due to their poor aqueous solubility, volatility, and limited stability. This study details the fabrication of an antibacterial system based on polycyclodextrin (PCD) network anchored to the surface of silver nanoparticles (NPs) (Ag/PCD nanostructure (NS)) for efficient loading and controlled delivery of carvacrol (CV), as a natural bioactive agent (Ag/PCD@CV). This system was characterized using FT-IR, XRD, TGA/DSC, FE-SEM, EDX mapping, zeta potential analysis and UV-Vis spectroscopy. *In vitro* release studies exhibited a sustained CV release behavior (~72 %) in Ag/PCD@CV NS over 48 h. Free radical scavenging activity increased from 21.6 ± 3.4 % in Ag NPs to 73.5 ± 3.4 % in Ag/PCD@CV, as measured by the DPPH assay, implying strong antioxidant potential of CV. The MTT assay using L929 fibroblasts demonstrated a reduction in the cytotoxicity of Ag NPs following PCD coating, while Ag/PCD@CV exhibited a cell viability of 72.3 ± 2.4 % under the studied conditions. Simultaneously, Ag/PCD@CV demonstrated enhanced antibacterial efficacy, showing approximately 56 % greater inhibition against *Staphylococcus aureus (S. aureus)*, compared to Ag/PCD. Overall, the results presented in this work demonstrate the potential of Ag/PCD@CV as a multifunctional bioactive delivery system, exhibiting sustained CV release, antioxidant activity, good cell viability, and enhanced antibacterial activity against *S. aureus*. These findings support further investigation of Ag/PCD@CV NS as a bioactive platform with antibacterial potential.

Keywords: Antimicrobial, Antioxidant, Silver Nanoparticles, Carvacrol, Polycyclodextrin

Journal Pre-proofs

1. Introduction

Bacteria, as a major component of the microbiota, are beneficial to the host. They are involved in mechanisms including modulating the metabolic phenotype, regulation of digestion, epithelium evolution, influencing the innate immune responses and preventing the colonization of opportunistic pathogens. However, bacterial infections, which could occur due to intrinsic and extrinsic parameters, disrupt the coexistence equilibrium between bacteria and the host [1,2]. This could lead to one of the major global health problems and exacerbate the prevalence of antibiotic resistant bacteria [3]. Considering this important issue, the World Health Organization (WHO) released a list of multidrug-resistant (MDR) pathogens such as *Staphylococcus aureus (S. aureus)* and *Escherichia coli (E. coli)* [4,5]. Consequently, given their ability to adapt and evade the effectiveness of diverse treatments while simultaneously transferring their resistance to other organisms, it becomes essential to search for alternative treatments against these bacteria [6]. The need to combat infections, especially those attributed to MDR bacteria, necessitates the development of new antibiotics and novel technological strategies for their delivery [7].

To address this challenge, nanotechnology has attracted the attention of microbiologists. It has emerged as a highly effective and beneficial therapeutic approach against microbes and offers significant potential due to its efficacy and remarkable therapeutic index [8,9]. With the development of nanotechnology, various types of nanomaterials with high antibacterial activity have received great attention in many fields. By changing their size, surface properties, or even the employed materials, nanoparticles (NPs) have emerged as promising platforms for antimicrobial applications and therapeutic delivery [10,11].

Among NPs, metallic NPs (MNPs), particularly zinc oxide (ZnO), copper oxide (CuO) and silver (Ag) NPs, have attracted considerable attention because of their distinctive physical, optical, chemical, and antibacterial properties. They could be synthesized by various procedures with the capability to tune their size, shape and morphology and could be modified using various agents [11,12]. Among

Journal Pre-proofs

them, Ag NPs, in particular, exhibit broad-spectrum antibacterial activity through direct interactions with bacterial cells, disruption of the cell wall and cytoplasmic membrane, interference with essential cellular processes, and generation of reactive oxygen species (ROS) [13,14]. Supported Ag-based nanostructures have also been investigated for biological applications. For example, Nazari et al. developed a γ-Fe_2O_3@C/PIDA nanostructure to stabilize Ag NPs and evaluated its bioactivity and antimicrobial performance [15]. However, their large specific surface area makes Ag NPs prone to aggregation, resulting in poor dispersibility and limited loading capability. To overcome these limitations, Ag NPs are functionalized by surface modification using non-toxic organic substances and biocompatible compounds like carbohydrates [16]. Cyclodextrins (CDs) are carbohydrate-based compounds that have been introduced as potential materials for the functionalization of Ag NPs. Andrade et al. reported βCD-coated Ag NPs in which βCD formed a stabilizing layer around the Ag NPs' surface, and the resulting NPs exhibited antibacterial activity against *E. coli* [17]. However, individual CD molecules contain isolated hydrophobic cavities and lack an extended architecture with multiple accessible host sites. Within this context, polycyclodextrins (PCDs) have been widely studied. They are crosslinked materials in which multiple CD cavities are integrated into a three-dimensional porous network. This architecture provides multiple host sites for hydrophobic compounds, while the oxygen-containing functional groups of PCDs can interact with Ag NPs surface [18-20]. These features make PCDs a promising platform for integrating Ag NPs with hydrophobic bioactive compounds [21].

Carvacrol (CV) is a monoterpenoid phenolic compound and a major constituent of essential oils (EOs) extracted from oregano, thyme, marjoram, and summer savory. It exhibits antimicrobial, antioxidant, anticancer, anti-inflammatory, immunomodulatory, and larvicidal activities, making it attractive for food and pharmaceutical industries [22,23]. However, its hydrophobicity, high volatility, strong odor, and limited stability restrict its practical use [24]. Inclusion complexation with βCD has therefore been investigated to improve the physicochemical properties of CV [25,26]. Trindade *et al.* reported a CV/βCD inclusion complex and demonstrated improved aqueous solubility

Journal Pre-proofs

and bioavailability of CV [27]. These findings highlight the potential of CD-based systems for the incorporation of CV and provide a rationale for extending this approach to crosslinked PCD networks.

Combining bioactive compounds with MNPs has been explored as a promising strategy for developing multifunctional systems with complementary antibacterial and therapeutic activities [28]. In particular, previous studies have investigated the functionalization of MNPs with CD-based systems and the use of CD inclusion complexes for CV delivery, demonstrating the potential of these approaches to improve antimicrobial performance and bioactive compound delivery [29,30]. However, these studies have mainly focused on conventional CD-based systems, in which individual CD molecules or CD-functionalized MNPs provide the host environment for CV. In contrast, the present approach employs a crosslinked PCD network in which multiple CD cavities are integrated into a porous three-dimensional polymeric architecture associated with Ag NPs, thereby providing a porous host architecture for the incorporation and controlled release of CV. To the best of our knowledge, such an Ag/PCD@CV nanostructure (NS), integrating Ag NPs and CV within a porous crosslinked PCD network, has not previously been reported.

In the present study, an Ag/PCD@CV NS was developed by forming a porous three-dimensional crosslinked PCD network in the presence of Ag NPs, using βCD as the monomer and Epiclon as the crosslinking agent. The oxygen-containing functional groups of the PCD network enabled its interaction with the Ag NPs' surface, while the CD cavities provided host sites for the subsequent incorporation of CV through host–guest interactions. The resulting NS was evaluated in terms of CV loading and release behavior, antioxidant activity, cytotoxicity, and antibacterial performance to assess its potential as a multifunctional bioactive delivery system.

2. Materials and methods

2.1. Chemicals

Silver nitrate (≥ 99.9 %, $AgNO_3$), Sodium borohydride (≥ 98.0 %, $NaBH_4$), Carvacrol (≥ 98.0 %,

Journal Pre-proofs

5-isopropyl-2-methylphenol, CV), β-cyclodextrin (≥ 97.0 %, βCD), Epiclon B-4400 (≥ 98.0 %, EPI), Triethylamine (≥ 99.5 %, Et_3N), Dimethyl sulfoxide (≥ 99.0 %, DMSO), methanol (≥ 99.5 %) and ethanol (≥ 99.5 %) were obtained from Merck (Darmstadt, Germany). Fetal bovine serum (FBS), Dulbecco's modified Eagle Medium (DMEM), (3-(4,5-dimethylthiazol-2-yl)-2,5-diphenyl tetrazolium bromide (MTT powder), 2, 2-diphenyl-1-picrylhydrazyl (DPPH), Ascorbic acid (AsA), Tween-80 (a non-ionic surfactant) and phosphate buffered saline powder (pH = 7.4, PBS) were purchased from Sigma–Aldrich (St. Louis, MO, USA). The strain of *S. aureus* ATCC 25923 was obtained from the persian type culture collection (Tehran, Iran). The L929 fibroblasts were purchased from the National Cell Bank of Iran (Pasteur Institute; Iran).

2.2. Synthesis of Ag NPs

The synthesis of Ag NPs was carried out using the chemical reduction approach [31]. Briefly, 10 ml of an aqueous solution of $AgNO_3$ (1 mM) was prepared and stirred at room temperature. Then, 30 ml of a freshly prepared $NaBH_4$ solution (2 mM) was poured dropwise to the latter solution under vigorous stirring for 30 min. The use of freshly prepared $NaBH_4$ ensured its effective reducing activity, while its dropwise addition under vigorous stirring promoted a relatively rapid and homogeneous reduction of Ag^+ ions throughout the reaction medium. These conditions favor the formation of Ag nuclei within a short period and helps limit uncontrolled subsequent particle growth and aggregation. The color gradually changed from colorless to distinct yellow, indicating the formation of reduced Ag NPs. The visual stability of the Ag NPs dispersion was also monitored immediately after synthesis and after 24 h of storage. No obvious macroscopic precipitation or visible aggregation was observed after 24 h (Fig. 1), supporting the stability of the synthesized Ag NPs over the observation period. The resulting precipitate was centrifuged at 11000 rpm for 10 min, washed three times with deionized (DI) water and dried under vacuum for 24 h. The final recovery yield of Ag NPs was approximately 90%.

Journal Pre-proofs



Fig. 1. Visual appearance of the Ag NPs dispersion immediately after synthesis (0 h, left) and after 24 h of storage (right).

2.3. Synthesis of Ag NPs coated with PCD (Ag/PCD NSs)

Firstly, Ag NPs (1 g) were dispersed in DMSO (10 ml). Then, βCD (1 mmol) and Et_3N (1 ml) were added to this dispersion. It was stirred at room temperature for 3 h. In the next step, EPI (8 mmol) was poured and the reaction was stirred for another 3 h. Ag NPs coated with PCD (Ag/PCD NSs) were collected by centrifugation at 9000 rpm for 10 min, washed with ethanol 3 times and dried under vacuum for 24 h [32]. The final recovery of the dried Ag/PCD NSs was approximately 70%.

2.4. Loading of CV into the Ag/PCD NSs (Ag/PCD@CV)

CV was loaded into Ag/PCD NSs according to the inclusion complexation (IC) method [33]. Briefly, 3 mg of Ag/PCD NSs were dispersed in PBS (1 ml, pH = 7.4). A solution of CV in ethanol (1 ml containing 2 mg of CV) was added dropwise to the suspension. The mixture was stirred at room temperature in the dark for 24 h to facilitate the incorporation of CV into the CDs cavities and PCD pores. The Final sample (Ag/PCD@CV) was isolated by centrifugation at 11,000 rpm for 10 min, washed with DI water to eliminate unloaded CV, and finally dried under vacuum for 24 h. To estimate CV loading efficiency and capacity, the content of the unloaded CV in the supernatant was measured from a calibration curve ($R^2 \geq 0.99$) of CV standard concentrations in ethanol solution using UV-Vis spectroscopy at 274 nm. CV loading ratios of the samples were calculated using the following

Journal Pre-proofs

equations (1 and 2):

$$\text{CV laoding efficiency (LE, \%)} = \frac{\text{mass of loaded CV}}{\text{mass of initial CV}} \times 100 \quad (1)$$

$$\text{CV loading capacity (LC, \%)} = \frac{\text{mass of loaded CV}}{\text{mass of final product}} \times 100 \quad (2)$$

2.5. In vitro CV release assay

The release profile of CV from Ag/PCD@CV NSs was assessed using the reported method [33]. 5 mg of Ag/PCD@CV was dispersed into 10 ml of PBS solution containing Tween-80 (0.1% w/v) at pH = 7.4. The release assay was carried out at 37 °C under dark condition by gentle shaking at 100 rpm. Sampling was performed at predetermined time intervals. At each time point, Ag/PCD@CV NSs were centrifuged at 11000 rpm for 10 min. 1 ml of the supernatant was replaced with an equal volume of fresh buffer solution to maintain sink conditions. The cumulative CV percentage release was determined by UV-Vis spectrophotometry (at 274 nm). A Standard solution of CV was applied to create the calibration curve of the released CV.

2.6. Antioxidant activity assessment

The DPPH free radical scavenging assay was applied to assess the antioxidant capacity of prepared samples, with AsA acting as a positive control and PBS serving as the negative control. Firstly, a 0.1 mM DPPH solution was prepared in methanol and stored in the dark condition. Then, 1.4 mg.ml^{-1} dispersions were prepared by dispersing the specimens in 4 ml of the DPPH solution. The solutions were thoroughly mixed and incubated in the dark for 120 min at room temperature. The absorbance at 517 nm was recorded using a microplate reader (Spectra Max Plus 384, Molecular Devices, USA) [34]. The percentage of inhibition of free radicals was calculated using the equation (3):

$$\text{DPPH scavenging (\%)} = \frac{(\text{Az} - \text{Ap})}{\text{Az}} \times 100 \quad (3)$$

Journal Pre-proofs

where A_z is the absorbance of the blank (DPPH solution without samples) and A_p is the absorbance of the sample.

For concentration-dependent evaluation, samples of Ag NPs and Ag/PCD@CV were obtained at different concentrations (0.2, 0.4, 0.6, 0.8, 1.0, 1.2, and 1.4 $mg.ml^{-1}$) in 4.0 ml of 0.1 mM DPPH solution. The mixtures were incubated under the same conditions, and absorbance was recorded in order to assess their capacity to scavenge radicals.

2.7. Cytotoxicity assay

The cytotoxicity of Ag, Ag/PCD and Ag/PCD@CV was tested by MTT assay using L929 fibroblast cells. L929 cells were cultured in DMEM with 10 % FBS and 1 % penicillin-streptomycin, and incubated at 37 °C in an atmosphere of 5% CO_2 for 24 h. Fresh medium containing the samples at doses of 10, 25, 50, 100 and 200 $\mu g.well^{-1}$ was then added to the wells, with a total volume of 200 µl per well. Untreated cells were defined as control wells and cell-free wells were used as blanks. Triplicate (n = 3) was used to test each condition. The plates were incubated at 37 °C for 48 h. After treatment, MTT reagent (0.5 $mg.ml^{-1}$) was added to each well and incubated for 4 h. Then, 100 µl of DMSO was added to each well and absorbance was read at 570 nm using a BioTek microplate reader (USA) [30]. Cell viability based on optical density (OD) was calculated via the following formula (4):

$$\text{Cell viability (\%)} = \frac{OD_S - OD_B}{OD_C - OD_B} \times 100 \quad (4)$$

where OD_S is absorbance of the samples, OD_B is absorbance of blank wells, and OD_C is absorbance of untreated control cells.

2.8. Antibacterial performance

The agar diffusion method was used to determine the antibacterial activity of CV, Ag, Ag/PCD, and Ag/PCD@CV against *S. aureus* ATCC 25923. A bacterial suspension (100 µL, 10^7 CFU ml^{-1})

Journal Pre-proofs

was inoculated onto the agar surface. Then 100 µL of each tested sample at the concentration of 1.4 mg ml^{-1} were deposited on the inoculated agar plates. Azithromycin was used as positive control and sterile DI water was used as negative control. Plates were incubated at 37 °C for 24 h. The antibacterial activity was determined by measuring the diameter of the inhibition zone in mm [35].

2.9. Statistical analysis

Statistical analysis was performed using GraphPad Prism 9.0.0 (GraphPad Software, La Jolla, CA, USA). Data are expressed as mean ± standard deviation (SD). Experiments were performed in triplicate (n = 3). For multiple comparisons among sample groups at a single concentration level, such as the DPPH scavenging activity and antibacterial inhibition zone assays, one-way analysis of variance (ANOVA) was performed, followed by Tukey's multiple-comparison post-hoc test. For DPPH and MTT assays that were concentration dependent, two-way ANOVA was used with sample/formulation type and concentration as two factors, followed by Tukey's multiple-comparison post-hoc test. The statistical significance was set as $*p < 0.05$, $**p < 0.01$, $***p < 0.001$ and $****p < 0.0001$.

2.10. Characterization instrument

Fourier Transform Infrared (FT-IR) spectra were recorded by KBr pellet method using a Magna 550 Nicolet FTIR spectrometer in the wavelength range of 400-4000 cm^{-1}. Thermogravimetric analysis (TGA) and Differential scanning calorimetry (DSC) results were achieved using SDT-Q600 V20.9 Build 20 instrument under inert condition at a heating rate of 10 °C min^{-1}. The X-ray diffraction (XRD) studies were carried out by a STOE Theta–theta PowderDiffraction System, radiation (1.54060 Cu), generator (40 kV, 40mA) in the range of $2\theta = 10°$ to 85°. Ultraviolet visible (UV–Vis) absorption spectra were measured with a Hewlett-Packard 8453 spectrometer (200–800 nm). The shape and size of the samples were characterized using field emission scanning electron microscope

Journal Pre-proofs

(FE-SEM, Tescan/Mira, Czech Republic). In order to identify the elemental composition, EDX Unit (Energy Dispersive X-ray Analyses) and elemental mapping were performed. The zeta potential was calculated using by a ZEN3600 Zetasizer (Malvern Instruments) in DI water at room temperature.

2. Results and discussion

As illustrated in Fig. 2, Ag NPs were synthesized through the chemical reduction method. The surface of the Ag NPs was coated and functionalized with a PCD polymeric network. PCD was obtained by the simple polymerization of βCD using EPI as a cross-linking agent. The abundant oxygenated groups within the PCD structure facilitated its attachment to and stabilization of the Ag NPs surface, resulting in the formation of the stable Ag/PCD NSs. Finally, CV, as a bioactive molecule, was incorporated into the cavities of the CD units and the porous PCD matrix through host–guest interactions and hydrogen bonding, respectively, resulting in the formation of Ag/PCD@CV.

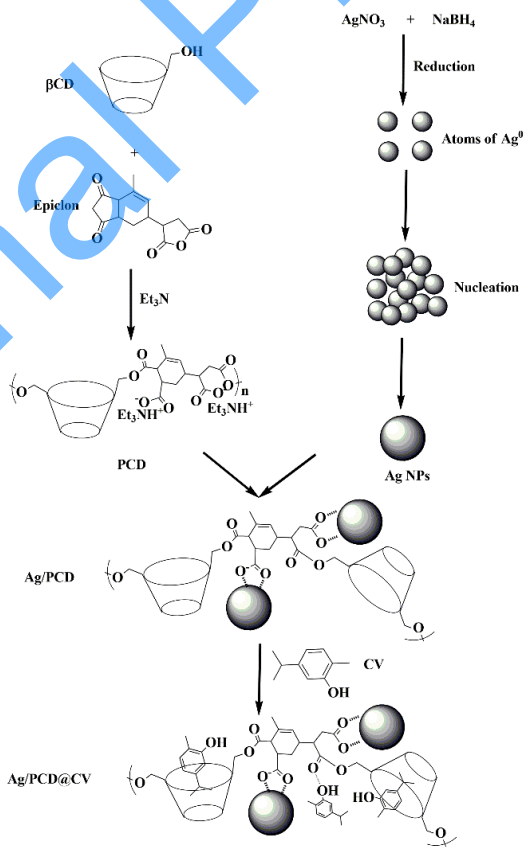


Fig. 2. Sequential steps for the preparation of Ag/PCD@CV NSs.

Journal Pre-proofs

3.1. FT-IR analysis

Fig. 3 shows the FT-IR spectra of CV, Ag NPs, free PCD, Ag/PCD and Ag/PCD@CV NSs. In the spectrum of Ag NPs (Fig. 3b), the intense and broad absorption bands in the range of 400-600 cm^{-1} were assigned to Ag-related vibrations, while the peaks centered at 3365 and 1635 cm^{-1} were attributed to the stretching and bending vibrations of O-H groups, respectively [36]. In the case of free PCD, two obvious peaks at 1735 and 1577 cm^{-1} were observed, corresponding to the carbonyl (C=O) ester bonds and carboxylate (COO^-) groups, respectively (Fig. 3c) [18] These bonds could be attributed to the linkage of the EPI anhydride rings as a crosslinking agent. The spectrum of Ag/PCD (Fig. 3d) exhibited a band at 1715 cm^{-1} corresponding to the carbonyl ester bonds in PCD. A slight shift to the lower frequencies was observed compared with bare PCD. This could be due to the interactions between Ag NPs and oxygenated functional groups of the PCD matrix [32]. Furthermore, the characteristic O–H stretching band of PCD at 3414 cm^{-1} shifted to 3345 cm^{-1} in Ag/PCD. This shift indicates a change in the hydrogen-bonding environment following the interaction of PCD with the Ag NPs. These interactions might play an important role in the stabilization and coating of the Ag NPs by the PCD. The spectrum of free CV (Fig. 3a) exhibited characteristic band at 1250 cm^{-1}, corresponding to the phenolic C-O stretching vibration. After CV incorporation, this band was markedly attenuated in the Ag/PCD@CV spectrum (Fig. 3e). Moreover, the O-H stretching band shifted from 3345 cm^{-1} in the Ag/PCD spectrum to 3334 cm^{-1} in the Ag/PCD@CV spectrum, indicating changes in the hydrogen-bonding environment due to interactions between the phenolic O-H group of CV and the hydroxyl groups of PCD [33].

3.2. XRD analysis

Crystallinity of Ag NPs and Ag/PCD NSs is investigated using X-ray diffraction technique. As shown in Fig. 4, the characteristic peaks of Ag NPs at 2θ = 38.98, 43.95, 65.71, 77.23 and 81.89 ° were attributed to the (111), (200), (220), (311) and (222) Bragg's planes, respectively. The results

Journal Pre-proofs

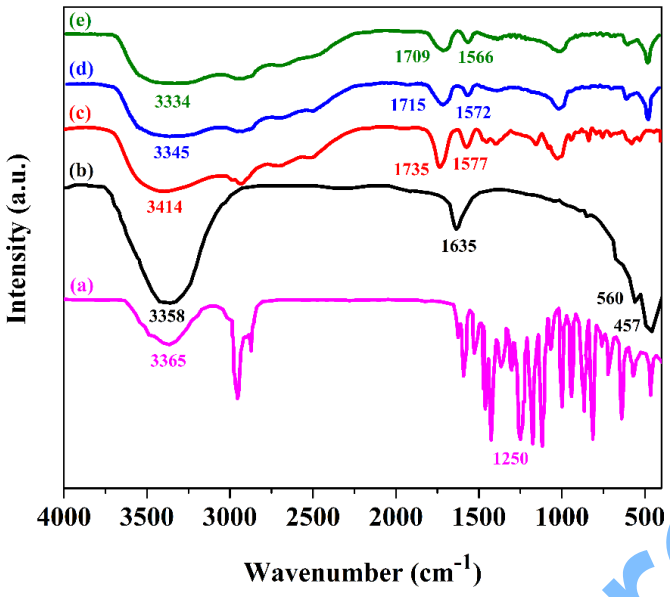


Fig. 3. FT-IR spectra of CV (a), Ag NPs (b), free PCD (c), Ag/PCD (d) and Ag/PCD@CV NSs (e).

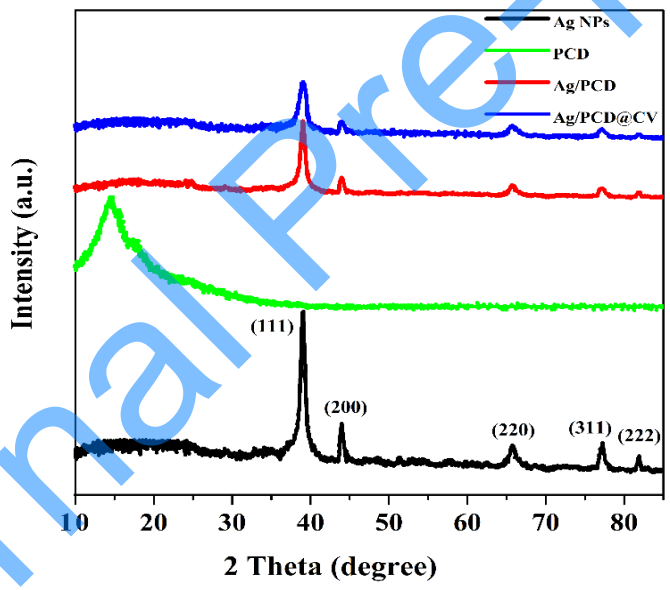


Fig .4. XRD patterns of Ag NPs, bare PCD, Ag/PCD and Ag/PCD@CV NSs.

are in good agreement with reflection patterns of JCPDS file no: 84-0713 corresponding to the face-centered cubic (fcc) structure of Ag NPs [37,38]. The Bragg diffraction angles remained intact in the case of Ag/PCD NSs, indicating preservation of the crystalline structure of Ag NPs during the surface modification process. Although, the reduced intensity of Ag peaks in Ag/PCD could be attributed to the presence of the amorphous PCD polymeric layer on the NPs surface. The characteristic diffraction

Journal Pre-proofs

pattern of Ag was also retained after CV loading in Ag/PCD@CV NSs, indicating that the incorporation of CV did not alter the crystalline structure of the Ag core. Moreover, no distinct additional crystalline diffraction peaks attributable to CV were observed in the Ag/PCD@CV pattern, suggesting that CV was not present as a separate crystalline phase and was likely dispersed within the PCD matrix [33,39].

3.3. TGA analysis

Fig. 5 indicates the weight loss curves of bare CV, Ag, Ag/PCD and Ag/PCD@CV. Pure Ag NPs showed a very limited weight loss of approximately 3.5 % below 200 °C, which could be attributed to the removal of physically adsorbed water molecules. The residual mass at 750 °C was approximately 94.3 %, illustrating the high thermal stability of Ag NPs [40]. In the case of Ag/PCD, two degradation stages were observed during thermal decomposition. An initial weight loss of approximately 5% was observed below 130 °C, which was due to the evaporation of surface moisture. The second mass reduction, of about 15 % occurred between 130 and 750 °C, corresponding to the degradation of the PCD network [32]. Bare CV exhibited a 97.0 % weight loss below 200 °C, indicating its poor thermal stability and rapid volatilization [41]. The TGA curve of Ag/PCD@CV illustrated significantly

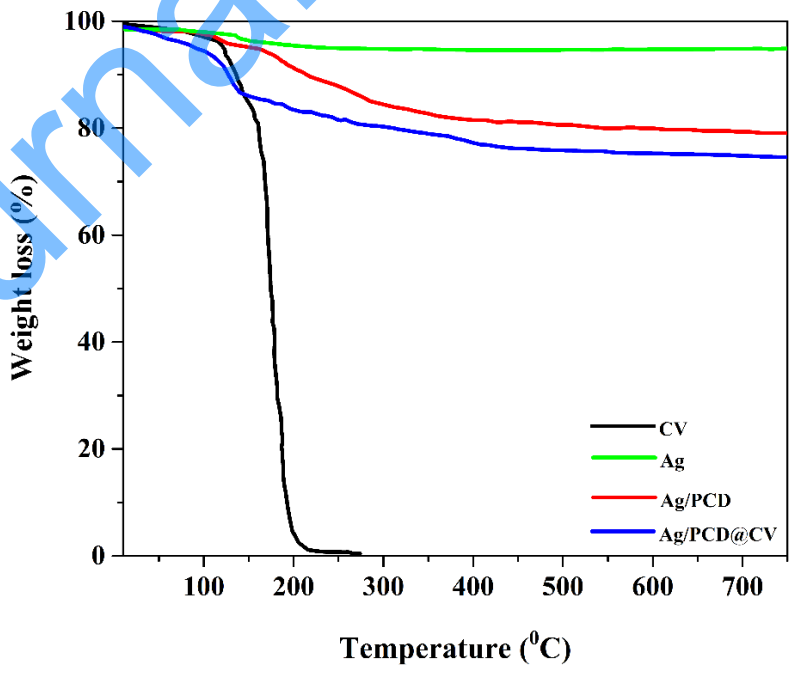


Fig. 5. TGA graphs of CV, Ag, Ag/PCD and Ag/PCD@CV NSs.

Journal Pre-proofs

thermal stability compared to CV. The first weight loss of about 13.4 % below 200 °C could be attributed to the dehydration and decomposition of encapsulated CV. The second weight loss of about 11.3 %, between 300 and 450 °C, might be due to the thermal destruction of the PCD shell located on the Ag NPs surface. The improved thermal stability of CV after encapsulation could be attributed to host–guest interactions and hydrogen bonding between CV molecules and the PCD matrix, which may restrict the volatilization and thermal decomposition of CV [42].

3.4. DSC analysis

The DSC thermograms of free CV, Ag/PCD and Ag/PCD@CV are shown in Fig. 6. Pure CV exhibited an intense negative peak at 244 °C. This endothermic peak corresponds to its volatilization and thermal decomposition [43]. For Ag/PCD, a broad endothermic peak centered around 120 °C was observed, which was due to the elimination of adsorbed water molecules and dehydration of oxygen-containing groups. Compared to pure CV, a remarkable reduction and broadening of the CV peak was observed around 170–220 °C. This phenomenon could be attributed to the restricted mobility of CV molecules after encapsulation [42]. The disappearance of the characteristic melting/endothermic transition of free CV supports the successful incorporation of CV within the Ag/PCD NS.

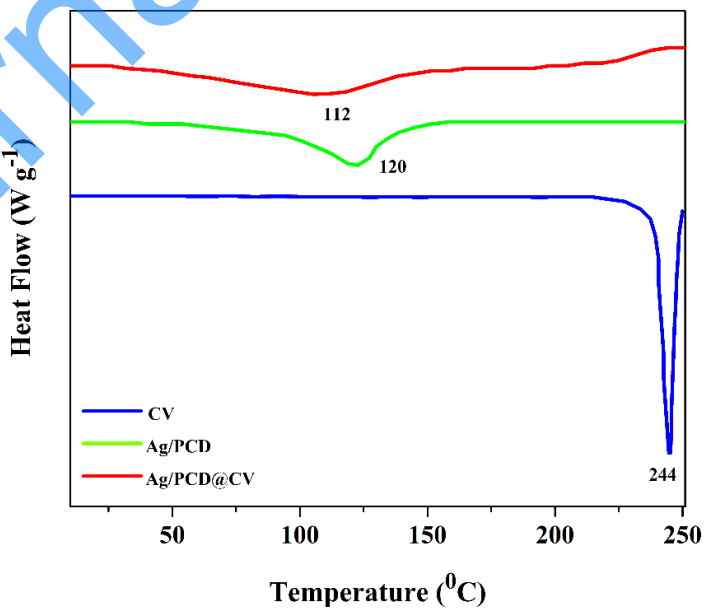


Fig. 6. DSC graphs of CV, Ag/PCD and Ag/PCD@CV NSs.

Journal Pre-proofs

3.5. Dynamic light scattering (DLS), Zeta potential, FE-SEM and elemental analyses

DLS measurement was applied for determination of hydrodynamic particle size distribution of Ag and Ag/PCD NSs. Mean diameter of Ag and Ag/PCD NSs were 54 and 76 nm, respectively. The low polydispersity index (PDI ≤ 0.2) of the prepared samples illustrated a proper size distribution, indicating the formation of uniform NSs. The zeta potential values of Ag, Ag/PCD, and Ag/PCD@CV NSs were determined to be −18.6±1.4, −34.2±1.4, and −25.1±1.5 mV, respectively (Fig. 7a) [44]. The negative surfae charge value of Ag/PCD was higher than that of nake Ag NPs. This could be attributed to the existence of the negatively hydroxyl and carboxyl functional groups of PCD network [32]. The zeta potential of Ag/PCD@CV was −25.1 mV indicating that negative charges of Ag/PCD was decreased by inclusion of CV molecules within the CD cavities and their interaction with the oxygenated groups of PCD [25]. Nevertheless, the negatively charged NPs have low tendency to agglomeartion, suggesting good colloidal stability of the Ag/PCD@CV nanosystem. Fig. 7b present the FE-SEM image of Ag/PCD NSs illustrating a spherical morphology with uniform size distribution [45]. The mean size of Ag/PCD NSs was determined 45 nm. However, there was a slight agglomeration, which might be caused after NPs coating by PCD polymeric shell.

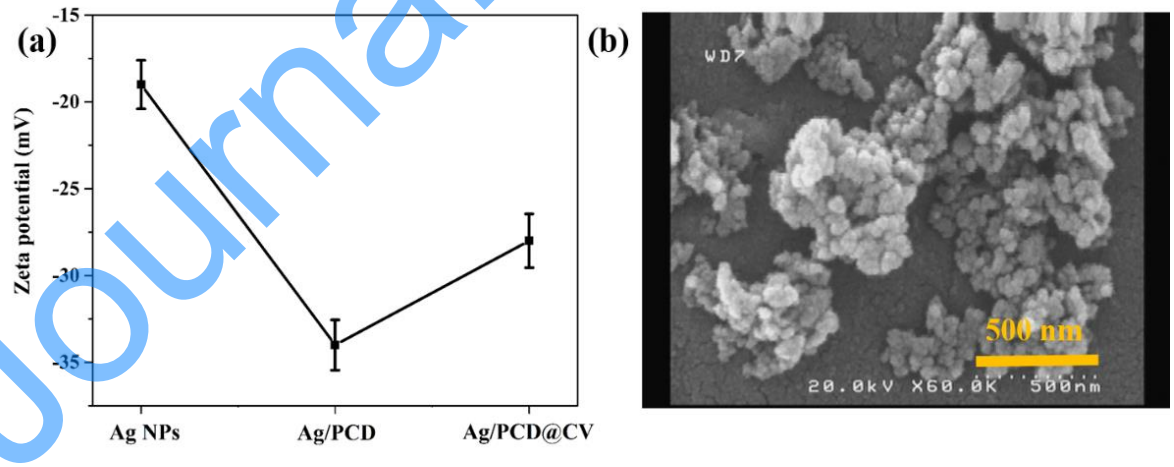


Fig. 7. Zeta potential diagram for prepared samples (a) and FE-SEM image of Ag/PCD NSs (b).

The EDX spectrum and elemental mapping of Ag/PCD NSs showed the presence of silver (82.0 %), carbon (8.1 %) and oxygen (9.9 %) elements (Fig. 8 (a and b)). The corresponding elemental

Journal Pre-proofs

mapping images further demonstrated the spatial distribution of Ag, C, and O throughout the NS, with a relatively uniform distribution of the detected elements and without obvious localized elemental segregation. These results support the successful formation of the Ag/PCD NSs and the relatively homogeneous distribution of PCD-associated elements around the Ag-based structure.

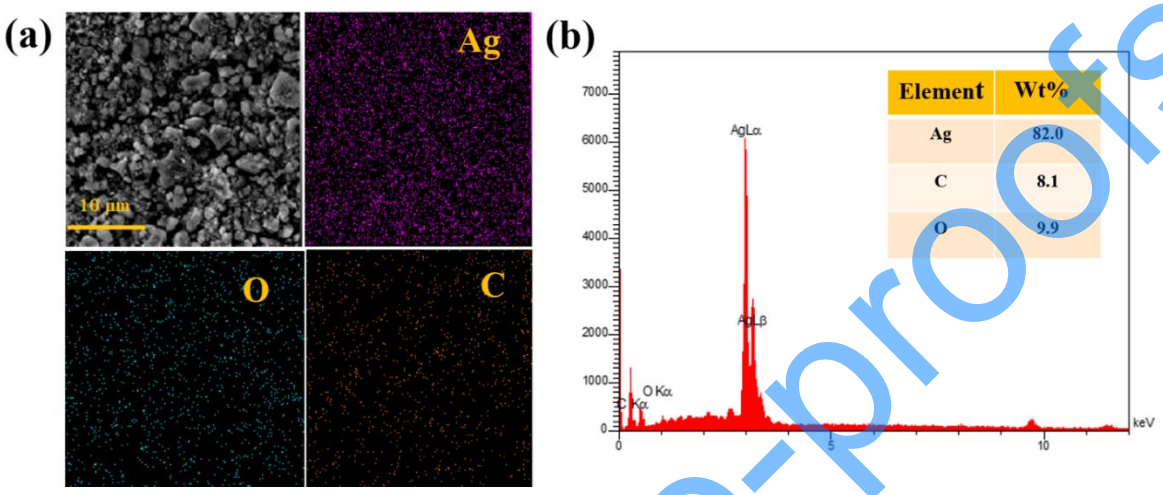


Fig. 8. Elemental mapping (a) and EDX spectrum of Ag/PCD NSs (b).

Taken together, the FT-IR, XRD, DLS, zeta potential, FE-SEM, and EDX results provide complementary evidence for the successful coating of Ag NPs with the PCD matrix. The shifts in the carbonyl and O–H bands, the increase in hydrodynamic size from 54 to 76 nm, the more negative zeta potential, and the presence and relatively uniform distribution of C and O around the Ag-based structure are consistent with the formation of a PCD coating on the Ag NPs.

3.6. Loading efficiency of CV

CV was loaded into the cone-shaped hydrophobic cavity of CD and the porous structure of the PCD polymeric network. The CV loading into the carrier could be attributed to the inclusion complex mechanism within the inner cavity of CD. Additionally, oxygen-containing groups of PCD could interact with the phenolic structure of CV through hydrogen bonding. The UV-Vis spectra of CV, Ag and Ag/PCD@CV are shown in Fig. 9. A characteristic peak at 425 nm was detected in the Ag NPs spectrum, which corresponds to the surface plasmon resonance of Ag NPs [46]. The characteristic

Journal Pre-proofs

absorption band at 274 nm was observed for the solution of free CV [47]. The intensity of the peak decreased in the case of Ag/PCD@CV, accompanied by a slight hypochromic effect, peak broadening, and a shift in the maximum absorption wavelength compared to free CV. These changes, particularly the restricted mobility of CV molecules within the CD cavities, provide supporting evidence for the incorporation of CV within the PCD network. This pattern is consistent with previous studies on guest–host interactions in CD-based nanocarriers [48]. In other words, the inclusion complex may shield the aromatic chromophore from surrounding media [49]. A slight shift in the maximum absorption wavelength was seen in the case of Ag/PCD@CV, implying that the electronic structure of CV remained unchanged without significant chemical degradation. CV loading efficiency and capacity were 88% and 26%, respectively, suggesting the potential of the system for pharmaceutical applications.

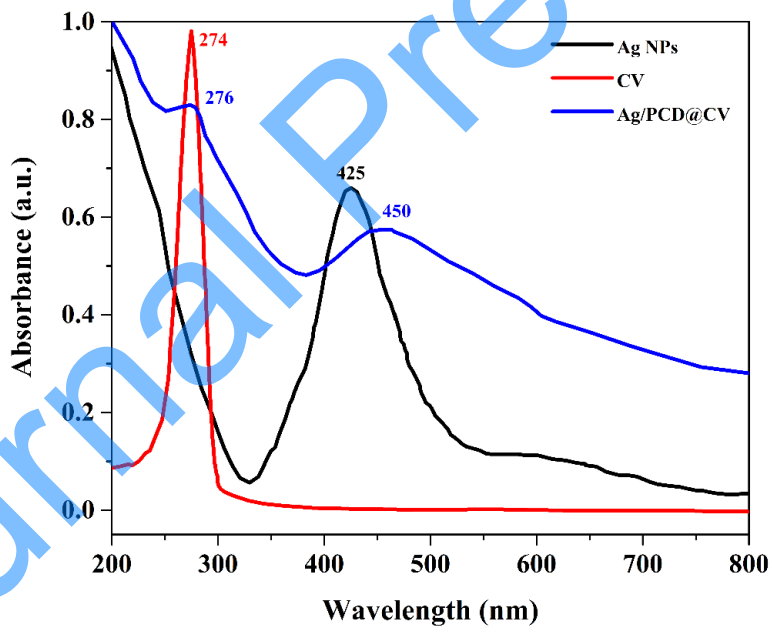


Fig. 9. UV-Vis spectra of CV, Ag and Ag/PCD@CV NSs.

3.7. In vitro CV Release study

The cumulative release profile of CV from Ag/PCD@CV was evaluated under physiological conditions and is presented in Fig. 10. The release pattern indicated a biphasic behavior characterized by an initial burst release followed by a sustained release phase. Firstly, CV was released from

Journal Pre-proofs

Ag/PCD@CV in neutral pH (about 40 % after 6 h). This phenomenon could be attributed to the diffusion of weakly adsorbed CV molecules from the carrier. Due to the controlled and prolonged release behavior, the release rate gradually declined. The cumulative release reached approximately 72% after 48 h. The hydrophilic nature of PCD layer could result in rapid hydration upon contact with aqueous media. As water penetrates into PCD polymeric matrix, it expands, thereby facilitating the diffusion the weakly entrapped CV. Therefore, a rapid burst release was observed in the early stages. A rapid initial release may be beneficial for the initial reduction of microbial burden and suppression of microbial viability. In the next phase, a slower and sustained release profile was observed. This pattern could be attributed to the formation of inclusion complex [50]. The encapsulated CV molecules within CD's cavities exhibited a slower diffusion rate from PCD network [51,52]. Furthermore, hydrogen bonding interactions between the phenolic structure of CV and the oxygenated groups of PCD might resulted in stronger retention of the CV within the system [53]. On the other hand, interactions between CV and the Ag NPs's surface could contribute to the slower release profile. Coordination interactions could limit molecular mobility, thereby delaying diffusion into the surrounding medium. These interactions could enhance the stability of the encapsulated CV and contribute to the prolonged release profile after the rapid phase. The prolonged release is desirable for maintaining antimicrobial activity over an extended period [54].

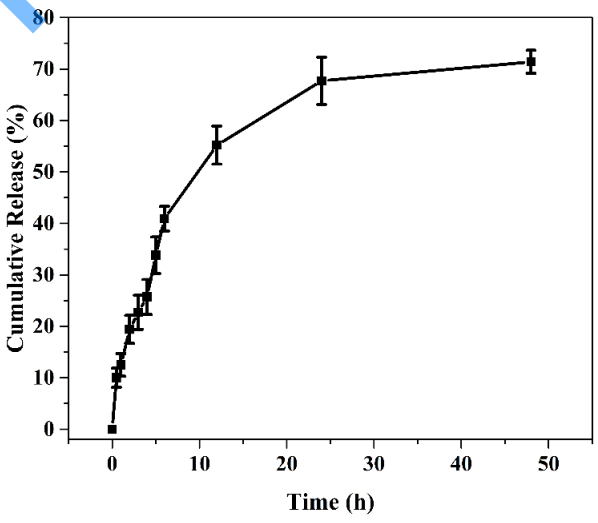


Fig. 10. Release profiles of CV from Ag/PCD@CV at pH = 7.4.

Journal Pre-proofs

For CV incorporation, the combined FT-IR, XRD, TGA, DSC, loading, and release results provide converging evidence for the association of CV within the PCD matrix through host–guest and hydrogen-bonding interactions. The changes in CV-related FT-IR bands and hydrogen-bonding environment, absence of a distinct crystalline CV phase, altered thermal behavior of CV, high loading capacity (26 %), and biphasic release profile collectively support CV incorporation within the PCD matrix rather than simple physical adsorption alone.

3.8. DPPH radical scavenging activity

Fig. 11a presents the DPPH radical scavenging efficiency of the samples. AgNPs exhibited relatively low scavenging activity (21.6 ± 3.4 %), which could be attributed to the limited inherent electron-donating capability of metallic NPs [55]. Ag/PCD NSs showed a slightly higher activity (37.9 ± 3.1 %) compared to bare Ag NPs, which may be related to the presence of carboxyl and hydroxyl groups on the PCD matrix. These functional groups could donate hydrogen atoms to neutralize free radicals and improve the dispersion of NPs in the media. However, due to the absence of strong radical-scavenging functional groups, the overall antioxidant contribution of the PCD layer is limited. Upon loading CV into the Ag/PCD NSs, a significant enhancement in DPPH radical scavenging activity was observed. The Ag/PCD@CV formulation illustrated a markedly higher scavenging efficiency (73.5 ± 3.2 %) in comparison with Ag (21.6 ± 3.4 %) and Ag/PCD NSs (37.9 ± 3.1 %) ($p < 0.05$). This enhancement is attributed to the presence of CV. It is a phenolic monoterpenoid with a hydroxyl group (OH) capable of donating hydrogen atoms for the neutralization of free radicals. The antioxidant capability of CV mainly proceeds via hydrogen atom transfer (HAT) and single-electron transfer (SET) processes. This leads to the formation of a resonance-stabilized phenoxyl radical, which prevents further oxidative damage [56]. Moreover, CV has been reported to enhance intracellular glutathione levels and may contribute to antioxidant defense through interactions with endogenous antioxidant systems [57,58]. In addition, the PCD

Journal Pre-proofs

matrix, with high capacity for CV loading, improved aqueous stability, and controlled release, plays a key role in enhancing the effective antioxidant performance of CV. The CV was loaded into the hydrophobic cavity of CD and the porous structure of PCD [52,59]. This phenomenon results in fewer active molecules of CV being directly accessible, which may reduce radical scavenging activity compared to free CV (83.6 ± 2.7). As shown in Figure 11b, a dose-dependent manner was observed in both bare Ag NPs and the Ag/PCD@CV formulation in DPPH radical scavenging activity. The Ag/PCD@CV efficiency increased from 41.3 ± 3.0 % (0.2 mg ml^{-1}) to 73.5 ± 3.2 % (1.4 $mg.ml^{-1}$). A similar but much weaker trend was seen in the case of Ag NPs (from 10.8 ± 1.9 % to 21.6 ± 3.4 %). These findings suggest that CV plays a crucial role in DPPH radical scavenging, supporting the strong antioxidant activity of the Ag/PCD@CV formulation [60].

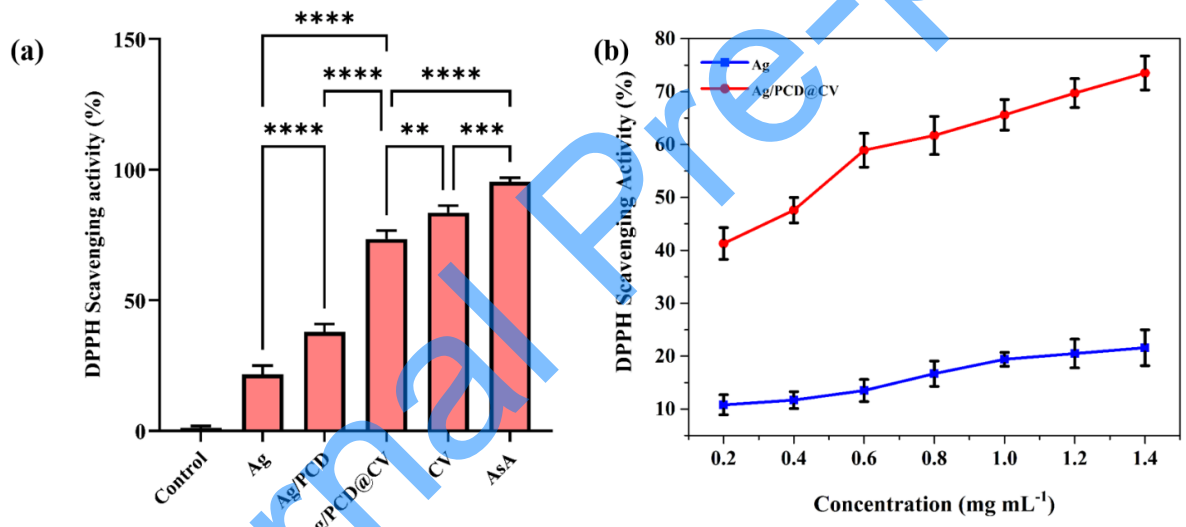


Fig. 11. DPPH Assay. Radical scavenging rate of samples (a) and Radical scavenging rate of Ag and Ag/PCD@CV at different concentrations (b).

3.9. Cytotoxicity analysis

The cytotoxicity of Ag, Ag/PCD and Ag/PCD@CV NSs was investigated in L929 fibroblast cells by MTT assay. Cell viability was determined after 48 h of exposure. As shown in Fig. 12, a dose-dependent response was observed for both pure Ag NPs and the functionalized formulations in the above cell line [61]. The Ag NPs displayed higher toxicity than Ag/PCD and Ag/PCD@CV NSs,

Journal Pre-proofs

with cell viability decreasing to approximately 22 % in L929 cells. This could be attributed to the intrinsic toxicity of Ag NPs, which can generate reactive oxygen species (ROS), release Ag^+ ions, and disrupt cellular membrane integrity. These effects induce oxidative stress and ultimately reduce cell viability [46,62,63]. A slight decrease in cell viability to about 72 % was observed in the case of Ag/PCD@CV. The relatively higher cytotoxicity of the Ag/PCD@CV formulation compared to Ag/PCD could be due to the concentration-dependent effects of CV on fibroblast cells and its gradual release from the PCD matrix. CV could induce oxidative stress and trigger apoptosis in mammalian cells via activation of the mitochondrial pathway [48]. However, the cell viability remained above 70 %, which is considered the standard acceptance limit according to ISO 10993-5. Therefore, Ag/PCD@CV demonstrated acceptable L929 fibroblast cell viability under the testing conditions, with cell viability persisting above 70 % at dosages up to 200 $\mu g.well^{-1}$ after 48 h of exposure.

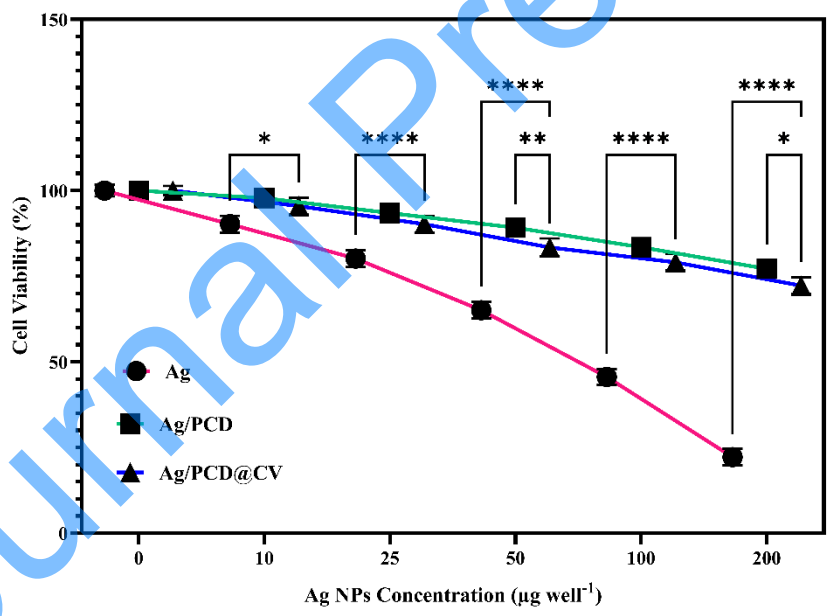


Fig. 12. MTT assay. Cell viability of samples after 48 h incubation for different concentration of Ag NPs**.**

3.10. Antimicrobial activity

The antibacterial activity of the prepared samples was evaluated against *S. aureus*, and the inhibition zones are shown in Fig. 13. The results demonstrated that bare Ag NPs exhibited an

Journal Pre-proofs

inhibition zone of 15.3 ± 0.6 mm, indicating their strong intrinsic antibacterial activity. Ag NPs can exert antibacterial effects through multiple mechanisms. Interaction with the bacterial cell membrane, interference with intracellular proteins and nucleic acids, release of Ag^+ ions and generation of ROS, are among the mechanisms that can contribute to bacterial cell death [64, 65]. Ag/PCD exhibited the smallest inhibition zone of 10.5 ± 0.6 mm. Decoration of Ag NPs with PCD network resulted in a significant decrease in the inhibition zone compared with bare Ag NPs. This reduction could be attributed to the coverage of the Ag NPs surfaces by the polymeric PCD layer, which may limit their direct interaction with bacterial cell surfaces and reduce the accessibility or release of Ag^+ ions. Although the PCD coating may reduce the antibacterial activity of bare Ag NPs, the MTT assay results indicated lower cytotoxicity of Ag/PCD toward L929 cells under the tested conditions.

Free CV demonstrated notable antibacterial activity against *S. aureus*, showing a larger inhibition zone than Ag/PCD (inhibition zone of 12.4 ± 0.3 mm). This is mainly attributed to the phenolic structure of CV. It disrupts the integrity of the bacterial cell wall, enhances membrane permeability, and leads to leakage of intracellular constituents. In addition, CV can interfere with membrane-associated proteins and cellular metabolic processes, thereby inhibiting bacterial growth [66-68]. Ag/PCD@CV exhibited the largest inhibition zone of 16.4 ± 0.6 mm , indicating an enhanced antibacterial effect against *S. aureus*. This enhanced activity may be attributed to the combined contribution of its components. Ag NPs generate ROS, which induce oxidative stress and damage essential cellular processes, while CV simultaneously interferes with membrane integrity. Furthermore, the PCD matrix acts as an efficient carrier for CV, improving its stability and enabling sustained release, thereby potentially contributing to prolonged antibacterial activity. Therefore, the larger inhibition zone observed for Ag/PCD@CV compared with the individual components suggests an enhanced antibacterial effect of the combined formulation. These findings are in agreement with previous reports demonstrating that the combined use of MNPs and bioactive phenolic compounds can enhance antibacterial efficacy compared with the individual components [69-71]. The enhanced

Journal Pre-proofs

antibacterial activity of Ag/PCD@CV against *S. aureus* supports the further investigation of this formulation for potential antimicrobial applications.

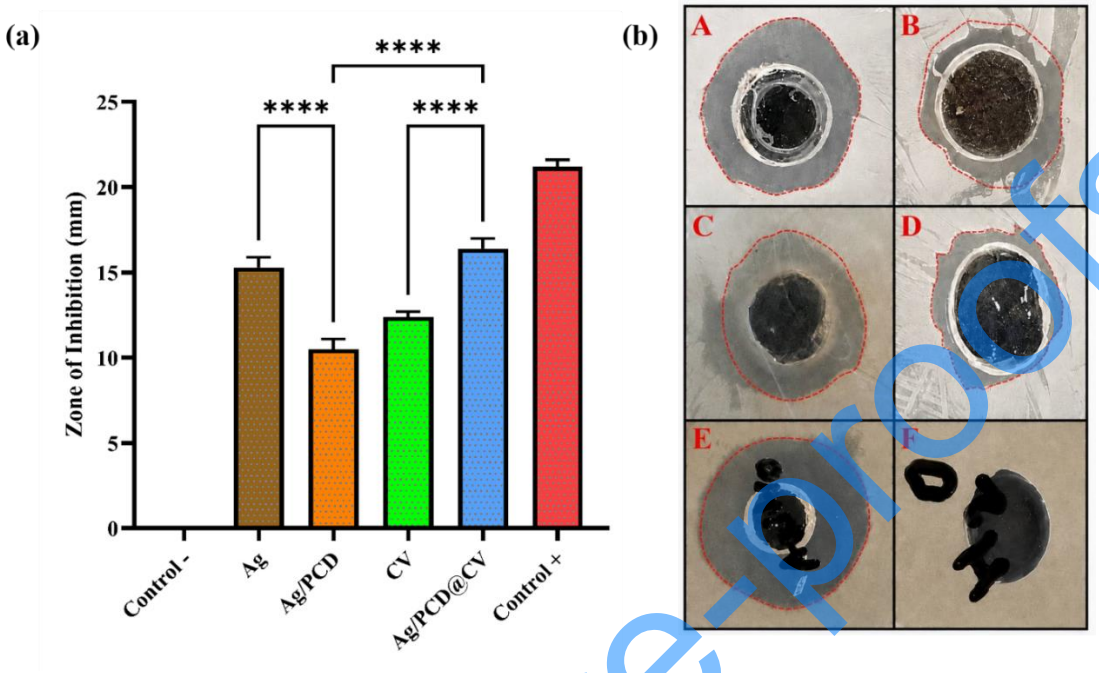


Fig. 13. Antimicrobial properties of the CV, Ag, Ag/PCD and Ag/PCD@CV. Quantitative results of the bacterial zone of inhibition (ZOI) diameter against *S.aureus* (a) and Photograph images of the ZOI against *S.aureus* (Ag (A), Ag/PCD (B), Ag/PCD@CV (C), CV (D), Control+ (E) and Control- (F) (b).

4. Conclusion

Based on the presented results, Ag/PCD@CV was successfully developed as a multifunctional bioactive NS for the efficient loading and controlled delivery of CV. The system exhibited sustained CV release (~72 % over 48 h), enhanced antioxidant activity, antibacterial activity against *S. aureus*, and a cell viability of 72.3 ± 2.4 % under the tested conditions. The developed concept integrates Ag NPs and CV within a crosslinked PCD network, where the porous three-dimensional PCD architecture provides both the inherent cavities of CD units and the porous structure of the crosslinked network for CV incorporation, while also contributing to the stabilization of Ag NPs. Compared with conventional Ag/CD and CD@CV systems, this integrated architecture combines the antibacterial properties of Ag with the antioxidant and bioactive properties of CV within a single PCD-based

Journal Pre-proofs

nanostructure. Further studies should focus on long-term stability and *in vivo* evaluation to further establish its potential for antibacterial and bioactive delivery applications.

Declaration of competing interest

The authors report no declarations of interest.

References

[1] Z. Ma, T. Zuo, N. Frey, A. Y. Rangrez, *Signal Transduction and Targeted Therapy*, 9 (2024) 237. https://doi.org/10.1038/s41392-024-01946-6

[2] M. G. Rooks, W. S. Garrett, Nature reviews. *Immunology*, 16 (2016) 341-352. https://doi.org/10.1038/nri.2016.42

[3] A. Nazir, A. Nazir, V. Zuhair, S. Aman, S. U. R. Sadiq, A. H. Hasan, M. Tariq, L. U. Rehman, M. J. Mustapha, D. B. Bulimbe, *Health Science Reports*, 8 (2025) e71077. https://doi.org/10.1002/hsr2.71077

[4] H. Sati, E. Carrara, A. Savoldi, P. Hansen, J. Garlasco, E. Campagnaro, S. Boccia, J.A. Castillo-Polo, E. Magrini, P. Garcia-Vello, E. Wool, V. Gigante, E. Duffy, A. Cassini, B. Huttner, P. R. Pardo, M. Naghavi, F. Mirzayev, M. Zignol, A. Cameron, E. Tacconelli, *The Lancet. Infectious Diseases*, 25 (2025) 1033-1043. https://doi.org/10.1016/s1473-3099(25)00118-5

[5] A. Marino, A. Maniaci, M. Lentini, S. Ronsivalle, G. Nunnari, S. Cocuzza, F. M. Parisi, B. Cacopardo, S. Lavalle, L. La Via, *Epidemiologia*, 6 (2025) 21. https://doi.org/10.3390/epidemiologia6020021

[6] A. B. Temesgen, S. A. Shiferaw, *BioMed Research International*, 2025 (2025) 8847267. https://doi.org/10.1155/bmri/8847267

[7] S. E. El-Sayed, A. A. Messiha, M. Zafer, *Journal of Infection and Public Health*, 19 (2026) 103058. https://doi.org/https://doi.org/10.1016/j.jiph.2025.103058

Journal Pre-proofs

[8] K. Pathak, M. Sarma, M. Sahariah, P. Shankarishan, J. J. Sahariah, S. Deka, A. Das, M. A. Islam, P. Pramanik, P. P. Borthakur, A. R. Bharadwaj, R. Bhaumik, *Next Nanotechnology*, 9 (2026) 100420. https://doi.org/https://doi.org/10.1016/j.nxnano.2026.100420

[9] L. Wang, C. Hu, L. Shao, *International Journal of Nanomedicine*, 12 (2017) 1227-1249. https://doi.org/10.2147/ijn.s121956

[10] D. M. AlQurashi, T. F. AlQurashi, R. I. Alam, S. Shaikh, M. A. M. *Tarkistani, Journal of Nanotheranostics*, 6 (2025) 9. https://doi.org/10.3390/jnt6020009

[11] F. Kurul, H. Turkmen, A. E. Cetin, S. N. Topkaya, *Next Nanotechnology*, 7 (2025) 100129. https://doi.org/https://doi.org/10.1016/j.nxnano.2024.100129

[12] A. Ribeiro, A. Dias, A. Zille, in, *ACS Applied Nano Materials*, 5 (2022) 3030–3064. https://doi.org/10.1021/acsanm.1c03891

[13] H. O. Khalifa, A. Oreiby, T. Mohammed, M. A. A. Abdelhamid, E. N. Sholkamy, H. Hashem, R. M. Fereig, *Frontiers in Cellular and Infection Microbiology*, 15 (2025) 1599113. https://doi.org/10.3389/fcimb.2025.1599113

[14] T. Bruna, F. Maldonado-Bravo, P. Jara, N. Caro, *International Journal of Molecular Sciences*, 22 (2021). https://doi.org/10.3390/ijms22137202

[15] S. Nazari, H. Alamgholiloo, E. Asgari, H. Rezakhani Moghaddam, H. Najafi Saleh, S. Parastar, A. Niapour, *Journal of Molecular Liquids*, 358 (2022) 119227. https://doi.org/10.3390/ijms22137202

[16] J. Liu, S. Legros, G. Ma, J. G. Veinot, F. Von der Kammer, T. Hofmann, *Chemosphere*, 87 (2012) 918-924. 10.1016/j.chemosphere.2012.01.045

[17] P. F. Andrade, A. F. de Faria, D. S. da Silva, J. A. Bonacin, M. D. C. Gonçalves, *Colloids and Surfaces B: Biointerfaces*, 118 (2014) 289-297. DOI: 10.1016/j.colsurfb.2014.03.032

[18] E. Gholibegloo, T. Mortezazadeh, F. Salehian, A. Ramazani, M. Amanlou, M. Khoobi, *Carbohydrate Polymers*, 213 (2019) 70-78. https://doi.org/https://doi.org/10.1016/j.carbpol.2019.02.075

Journal Pre-proofs

[19] S. Salazar Sandoval, T. Bruna, F. Maldonado-Bravo, K. Bolaños, S. Adasme-Reyes, A. Riveros, N. Caro, N. Yutronic, N. Silva, M.J. Kogan, P. Jara, *Materials* (Basel), 16 (2023). https://doi.org/10.3390/ma16093538

[20] A. Di Vincenzo, D. Chillura Martino, E. Piacenza, P. Conte, A. Pettignano, G. Lazzara, P. Lo Meo, *Applied Surface Science Advances*, 15 (2023) 100407. https://doi.org/https://doi.org/10.1016/j.apsadv.2023.100407

[21] O.E. Nicolaescu, C. Ionescu, A. Samide, C. Tigae, C.I. Spînu, B. Oprea, *Pharmaceutics,* 17 (2025). https://doi.org/10.3390/pharmaceutics17040506

[22] M. Sharifi-Rad, E.M. Varoni, M. Iriti, M. Martorell, W.N. Setzer, M. Del Mar Contreras, B. Salehi, A. Soltani-Nejad, S. Rajabi, M. Tajbakhsh, J. Sharifi-Rad, *Phytotherapy Research : PTR*, 32 (2018) 1675-1687. https://doi.org/10.1002/ptr.6103

[23] A. Nostro, T. Papalia, *Recent Patents on Anti-Infective Drug Discovery*, 7 (2012) 28-35. https://doi.org/10.2174/157489112799829684

[24] A. Maurya, A. Yadav, M. Soni, K.K. Paul, U. Banjare, M.K. Jha, A.K. Dwivedy, N.K. Dubey, *Foods* (Basel, Switzerland), 13 (2024). https://doi.org/10.3390/foods13244013

[25] S. Pedotti, G. Ginestra, G. Granata, L. Ferreri, G. Gambera, S. Petralia, F. Ruffino, M.F. Taviano, A. Nostro, G.M.L. Consoli, *Carbohydrate Polymers*, 372 (2026) 124540. https://doi.org/https://doi.org/10.1016/j.carbpol.2025.124540

[26] S. Peimanfard, A. Zarrabi, F. Trotta, A. Matencio, C. Cecone, F. Caldera, *Pharmaceutics,* 14 (2022). https://doi.org/10.3390/pharmaceutics14051059

[27] G.G.G. Trindade, G. Thrivikraman, P.P. Menezes, C.M. França, B.S. Lima, Y. Carvalho, E. Souza, M.C. Duarte, S. Shanmugam, L.J. Quintans-Júnior, D.P. Bezerra, L.E. Bertassoni, A.A.S. Araújo, *Food and chemical toxicology : an international journal published for the British Industrial Biological Research Association*, 125 (2019) 198-209. https://doi.org/10.1016/j.fct.2019.01.003

[28] A.I. Ribeiro, A.M. Dias, A. Zille, *ACS applied nano materials*, 5 (2022) 3030-3064.

Journal Pre-proofs

https://doi.org/10.1021/acsanm.1c03891

[29] E.V. Campos, P.L. Proença, J.L. Oliveira, A.E. Pereira, L.N. de Morais Ribeiro, F.O. Fernandes, K.C. Gonçalves, R.A. Polanczyk, T. Pasquoto-Stigliani, R. Lima, *Scientific reports*, 8 (2018) 7623. https://doi.org/10.1038/s41598-018-26043-x

[30] Y. Wu, L. Yang, G. Shi, L. Zou, J. He, J. Li, A. Zhang, X. Wang, Z. Liu, K. Tang, *International Journal of Biological Macromolecules*, 291 (2025) 139126. 10.1016/j.ijbiomac.2024.139126

[31] V.S. Chandak, P.V. Nagime, *Hybrid Advances*, 8 (2025) 100389. https://doi.org/https://doi.org/10.1016/j.hybadv.2025.100389

[32] E. Gholibegloo, T. Mortezazadeh, F. Salehian, H. Forootanfar, L. Firoozpour, A. Foroumadi, A. Ramazani, M. Khoobi, *Journal of colloid and interface science*, 556 (2019) 128-139. https://doi.org/https://doi.org/10.1016/j.jcis.2019.08.046

[33] K. Ates, Z.I. Yildiz, *Journal of Food Engineering*, 391 (2025) 112445. 10.1016/j.jfoodeng.2024.112445

[34] K. Ertan, A. Celebioglu, R. Chowdhury, G. Sumnu, S. Sahin, C. Altier, T. Uyar, *Food Hydrocolloids*, 142 (2023) 108864. 10.1016/j.foodhyd.2023.108864

[35] H. Zomorrodian, A. Abedi, M. Arbabi, R. Gholampour, M. Abedi, H. Schonherr, E. Gholibegloo, M. Raoufi, *International Journal of Biological Macromolecules*, (2025) 149640. 10.1016/j.ijbiomac.2025.149640

[36] S. Bhattacharjee, G. Debnath, A.R. Das, A.K. Saha, P. Das, *Advances in Natural Sciences: Nanoscience and Nanotechnology*, 8 (2017) 045008. 10.1088/2043-6254/aa84ec

[37] S.N. Fakher, F.J. Kashi, *Journal of Inorganic and Organometallic Polymers and Materials*, 31 (2021) 1688-1703. https://doi.org/10.1007/s10904-021-01879-5

[38] M.H. Ali, M.A.K. Azad, K.A. Khan, M.O. Rahman, U. Chakma, A. Kumer, *ACS omega*, 8 (2023) 28133-28142. https://doi.org/10.1021/acsomega.3c01261

[39] Z. Cao, J. Su, Y. Luo, X. Wang, Z. Liu, Y. Chen, Y. Zou, W. Shen, X. Ge, *Food and Bioprocess*

Journal Pre-proofs

Technology, 18 (2025) 1580-1600. https://doi.org/10.1007/s11947-024-03524-8

[40] K.W. Fan, A.M. Granville, *Polymers,* 8 (2016) 81. https://doi.org/10.3390/polym8030081.

[41] S. Hendessi, E.B. Sevinis, S. Unal, F.C. Cebeci, Y.Z. Menceloglu, H. Unal, *Progress in Organic Coatings*, 101 (2016) 253-261. https://doi.org/https://doi.org/10.1016/j.porgcoat.2016.09.005

[42] Y. Liu, L. Weng, Y. Lin, D. Lin, L. Xie, T. Zhong, *Heliyon*, 9 (2023) e18804. https://doi.org/https://doi.org/10.1016/j.heliyon.2023.e18804

[43] A. Tópor, F. F. Veras, F. A. Cacciatore, R. D. Silveira, P. da Silva Malheiros, J. E. Welke, *International Journal of Food Microbiology*, 416 (2024) 110659. https://doi.org/https://doi.org/10.1016/j.ijfoodmicro.2024.110659

[44] J. Xu, M. Yıldıztekin, D. Han, C. Keskin, A. Baran, M. F. Baran, A. Eftekhari, C. A. Ava, S.İ. Kandemir, D. B. Cebe, B. Dağ, A. Beilerli, R. Khalilov, *Heliyon*, 9 (2023) e19061. https://doi.org/https://doi.org/10.1016/j.heliyon.2023.e19061

[45] S. M. Alsharif, S.S. Salem, M. A. Abdel-Rahman, A. Fouda, A. M. Eid, S. El-Din Hassan, M. A. Awad, A. A. Mohamed, *Heliyon*, 6 (2020) e03943. https://doi.org/https://doi.org/10.1016/j.heliyon.2020.e03943

[46] A. Sati, T. N. Ranade, S. N. Mali, H. K. Ahmad Yasin, A. Pratap, *ACS Omega,* 10 (2025) 7549-7582. https://doi.org/10.1021/acsomega.4c11045

[47] H. Hajimehdipoor, M. Shekarchi, M. Khanavi, N. Adib, M. Amri, *Pharmacognosy magazine*, 6 (2010) 154-158. https://doi.org/10.4103/0973-1296.66927

[48] K. A. D. Roy, S. S. Desai, P. Abishad, A. K. Ahalya, R. Krishnan, V. K. Vinod, A. Karthikeyan, K. Rajagopal, R. Nayar, S. B. Barbuddhe, D. B. Rawool, J. Vergis, *Results in Surfaces and Interfaces*, 19 (2025) 100565. https://doi.org/https://doi.org/10.1016/j.rsurfi.2025.100565

[49] L. Higueras, G. López-Carballo, R. Gavara, P. Hernández-Muñoz, *Food Hydrocolloids*, 43 (2015) 603-611. https://doi.org/https://doi.org/10.1016/j.foodhyd.2014.07.017

[50] Á. Sarabia-Vallejo, M. d. M. Caja, A. I. Olives, M. A. Martín, J.C. Menéndez, *Pharmaceutics*,

Journal Pre-proofs

15 (2023) 2345. https://doi.org/10.3390/pharmaceutics15092345

[51] D. O. de Castro, N. Tabary, B. Martel, A. Gandini, N. Belgacem, J. Bras, *Cellulose*, 25 (2018) 1249-1263. https://doi.org/10.1007/s10570-017-1646-6

[52] E. V. R. Campos, P. L. F. Proença, J. L. Oliveira, A. E. S. Pereira, L. N. de Morais Ribeiro, F. O. Fernandes, K. C. Gonçalves, R.A. Polanczyk, T. Pasquoto-Stigliani, R. Lima, C.C. Melville, J.F. Della Vechia, D. J. Andrade, L. F. Fraceto, *Scientific Reports*, 8 (2018) 7623. https://doi.org/10.1038/s41598-018-26043-x

[53] F. Topuz, T. Uyar, Pharmaceutics, 11 (2018) 6. https://doi.org/10.3390/pharmaceutics11010006

[54] A. Nair, R. Mallya, V. Suvarna, T. A. Khan, M. Momin, A. Omri, *Antibiotics* (Basel), 11 (2022). https://doi.org/10.3390/antibiotics11010108

[55] H. Rizwana, R. M. Aljowaie, F. Al Otibi, M. S. Alwahibi, S. A. Alharbi, S. A. Al asmari, N. S. Aldosari, H. A. Aldehaish, *Scientific Reports*, 13 (2023) 16270. https://doi.org/10.1038/s41598-023-43384-4

[56] J. Wang, L. Zhao, W. Tian, H. Zhang, P. Wang, Q. Zhan, H. Fan, X. Yu, LWT, 212 (2024) 117035. https://doi.org/https://doi.org/10.1016/j.lwt.2024.117035

[57] M.M. Abu-Serie, N.H. Habashy, W.E. Attia, *BMC Complementary and Alternative Medicine*, 18 (2018) 154. https://doi.org/10.1186/s12906-018-2218-5

[58] T. Benincá, L. Schmidt, L. Thomé Cardoso, P. Rossini Augusti, P. da Silva Malheiros, *Food Research International*, 197 (2024) 115256. https://doi.org/https://doi.org/10.1016/j.foodres.2024.115256

[59] A. Rezaei, S. Khavari, M. Sami, *Journal of Molecular Structure*, 1241 (2021) 130610. https://doi.org/https://doi.org/10.1016/j.molstruc.2021.130610

[60] G. I. Potra Cicalău, G. Ciavoi, I. Scrobotă, A. O. Marcu, I. Romanul, E. Marian, L. vG. Vicaș, M. Ganea, *Dentistry Journal* (Basel), 11 (2023) 284. https://doi.org/10.3390/dj11120284

[61] S. Kumar, P. Masurkar, B. Sravani, D. Bag, K. R. Sharma, P. Singh, T. Korra, M. Meena, P.

Journal Pre-proofs

Swapnil, V. D. Rajput, T. Minkina, *Journal of Nanoparticle Research*, 25 (2023) 54. https://doi.org/10.1007/s11051-023-05708-3

[62] O. Bondarenko, K. Juganson, A. Ivask, K. Kasemets, M. Mortimer, A. Kahru, *Archives of Toxicology,* 87 (2013) 1181-1200. https://doi.org/10.1007/s00204-013-1079-4

[63] K. C. Nguyen, V. L. Seligy, A. Massarsky, T. W. Moon, P. Rippstein, J. Tan, A. F. Tayabali, *Journal of Physics: Conference Series*, 2013, pp. 012025. 10.1088/1742-6596/429/1/012025

[64] M. -S. Wong, C. -W. Chen, C. -C. Hsieh, S. -C. Hung, D. -S. Sun, H. -H. Chang, *Scientific Reports*, 5 (2015) 11978. https://doi.org/10.1038/srep11978

[65] A. Nasir, I. H. Sajid, A. Syed, F. Adnan, S. Rizwan, *Nano-Structures & Nano-Objects*, 40 (2024) 101415. https://doi.org/https://doi.org/10.1016/j.nanoso.2024.101415

[66] W. Mączka, M. Twardawska, M. Grabarczyk, K. Wińska, *Antibiotics* (Basel), 12 (2023). https://doi.org/10.3390/antibiotics12050824

[67] A. Ultee, M.H. Bennik, R. Moezelaar, *Appl Environ Microbiol*, 68 (2002) 1561-1568. https://doi.org/10.1128/aem.68.4.1561-1568.2002

[68] C. Zhang, Z. Li, D. Hu, *Journal of Drug Delivery Science and Technology*, 97 (2024) 105779. https://doi.org/https://doi.org/10.1016/j.jddst.2024.105779

[69] S. Scandorieiro, F. Teixeira, M. C. L. Nogueira, L. A. Panagio, A.G. de Oliveira, N. Durán, G. Nakazato, R. K. T. Kobayashi, *Antibiotics* (Basel), 12 (2023). https://doi.org/10.3390/antibiotics12040756

[70] L. Pinto, F. Baruzzi, R. Terzano, F. Busto, A. Marzulli, C. Magno, S. Cometa, E. De Giglio, *Molecules*, 29 (2024) 3607. https://doi.org/10.3390/molecules29153607

[71] V. Vilas, D. Philip, J. Mathew, *Journal of Molecular Liquids*, 221 (2016) 179-189. https://doi.org/https://doi.org/10.1016/j.molliq.2016.05.066

Journal Pre-proofs